Sonochemical synthesis and characterization of Ag/AgCl/Bi_2MoO_6 as visible-light-driven photocatalyst for rhodamine B degradation

A. Phuruangrat[a,*], R. Dumkaew[a], B. Kuntalue[b], T. Sakhon[b], T. Thongtem[c, d], S. Thongtem[c, e]

[a] *Division of Physical Science, Faculty of Science, Prince of Songkla University, Hat Yai, Songkhla 90112, Thailand*

[b] *Electron Microscopy Research and Service Center, Faculty of Science, Chiang Mai University, Chiang Mai 50200, Thailand*

[c] *Materials Science Research Center, Faculty of Science, Chiang Mai University, Chiang Mai 50200, Thailand*

[d] *Department of Chemistry, Faculty of Science, Chiang Mai University, Chiang Mai 50200, Thailand*

[e] *Department of Physics and Materials Science, Faculty of Science, Chiang Mai University, Chiang Mai 50200, Thailand*

Heterostructure Ag/AgCl/Bi_2MoO_6 nanocomposites as visible-light-driven photocatalyst for rhodamine B (RhB) degradation were prepared by precipitation and sonochemical-assisted deposition method. The phase, morphology, oxidation state of element and optical properties of heterostructure Ag/AgCl/Bi_2MoO_6 nanocomposites were characterized by X-ray diffraction (XRD), scanning electron microscopy (SEM), X-ray photoelectron spectroscopy (XPS) and UV-visible spectroscopy. In this research, the pure sample prepared by simple hydrothermal method was orthorhombic phase of Bi_2MoO_6 nanoplates with smooth surfaces. Upon being loaded with Ag/AgCl by sonochemical-assisted deposition method, AgCl and Ag nanoparticles were deposited on the surface of Bi_2MoO_6 nanoplates. The UV-visible spectra of Ag/AgCl/Bi_2MoO_6 nanocomposites show visible light absorption higher than pure Bi_2MoO_6 nanoplates. The enhanced photocatalytic efficiency of Ag/AgCl/Bi_2MoO_6 nanocomposites was investigated through rhodamine B (RhB) degradation under visible light irradiation and compared with those of the Bi_2MoO_6 nanoplates and AgCl/Bi_2MoO_6 nanocomposites. The photocatalytic efficiency of heterostructure Ag/AgCl/Bi_2MoO_6 nanocomposites in degrading RhB under visible light irradiation is higher than those of Bi_2MoO_6 nanoplates and AgCl/Bi_2MoO_6 nanocomposites. The photocatalytic efficiency of Ag/AgCl/Bi_2MoO_6 nanocomposites in degrading RhB is 99.70% under visible light irradiation within 30 min.

(Received December 8, 2021; Accepted February 15, 2022)

Keywords: Ag/AgCl/Bi_2MoO_6; Stable photocatalyst; XRD

1. Introduction

Contamination of organic pollutants in water released from textile, medicine, plastic and other industries is one of the most serious problems for environmental sustainable development and human health [1-5]. Photocatalysis as an advanced oxidation and green process is an effective and potential method used for removal of many toxic organic pollutants from aqueous system because of its low cost, simplicity and high efficiency [4, 6, 7]. The photocatalytic process is induced by photonic energy to produce radicals and photogenerated holes with a strong oxidation ability to degrade pollutants

* Corresponding author: phuruangrat@hotmail.com
https://doi.org/10.15251/DJNB.2022.171.209

[6, 8-10]. Comparing to the traditional treatment method, photocatalytic technology has the advantage of low energy consumption, simple operation, mild reaction condition and no formation of secondary pollution [3, 4, 6]. Therefore, photocatalytic degradation of organic pollutants is preferable as a feasible wastewater treatment strategy.

Orthorhombic Bi_2MoO_6 material as Aurivillius layer structure with a small bandgap (2.40–2.75 eV) is composed of layered structure with the perovskite-like slabs of MoO_6 sandwiched between $(Bi_2O_2)^{2+}$ layers. The material has been widely used in many potential applications such as gas sensing, ion-conductive, luminescent, dielectric and catalytic application [2, 11, 12]. It is an excellent photocatalyst for degradation of organic pollutants and water splitting under visible light irradiation [2, 11-13]. Hence, the practical application of Bi_2MoO_6 is limited by low quantum yield and fast recombination of photo-induced charge carriers [2, 11, 12, 14]. At present, plasmonic photocatalytic system has been adopted to improve photocatalytic performance [1, 13, 15]. Ag/AgCl nanoparticles are able to efficiently absorb visible light due to the surface plasmon resonance (SPR) effect of metallic Ag formed by photoreduction of AgCl [1, 15, 16]. The junction between Ag and AgCl leads to efficient separation of photogenerated electron-hole pairs and enhance the photocatalytic performance [1, 13, 16]. In previous literatures, Ag/AgCl coupled with semiconductor photocatalyst such as $Ag/AgCl/WO_3$ [17], $Ag/AgCl/ZnTiO_3$ [18], $Ag/AgCl/Bi_2Zr_2O_7$ [19] and $Ag/AgCl/ZnCo_2O_4$ [20] shows enhanced photocatalytic activity for dye degradation under visible light irradiation due to an integration of the synergetic effect of suitable size plasmonic Ag/AgCl and strong coupling effect between Ag@AgCl and semiconductor photocatalyst [13, 16, 18, 20, 21]. This synergetic effect is superior for visible-light-responsive, fast separation of electron–hole pairs and enhancing the photocatalytic reaction [16, 21, 22].

In this paper, $Ag/AgCl/Bi_2MoO_6$ nanocomposites were prepared by precipitation and sonochemical deposition method. The structure, morphology, composition and optical property of as-prepared photocatalyst were characterized by various analytical techniques. The photocatalytic performance of the prepared photocatalyst was monitored by rhodamine B (RhB) as dye model under visible light irradiation. Active radicals of the process were also investigated in this research.

2. Experiment

Pure thin Bi_2MoO_6 nanoplates were synthesized by hydrothermal method. Typically, each 0.01 mole of $Bi(NO_3)_3{\cdot}5H_2O$ and 0.005 mole of Na_2MoO_4 were weighted and dissolved in 100 ml reverse osmosis (RO) water under continued stirring at room temperature. Then, it was adjusted the pH to 6 by 3 M NaOH to form a white suspension solution and transferred into a 200 mL Teflon-lined stainless steel autoclave. The stainless-steel autoclave was sealed and heated at 180 ^oC for 20 h in an electric oven. Then, the as-prepared Bi_2MoO_6 precipitates were collected, washed and dried for further preparing of $Ag/AgCl/Bi_2MoO_6$ nanocomposites by precipitation–sonochemical deposition method.

To prepare heterostructure 5% $AgCl/Bi_2MoO_6$ heterojunctions, 5% $AgNO_3$ and NaCl by weight were weighted and dissolved in 20 ml RO water. The two solutions were put in 2.5 g Bi_2MoO_6 suspension and vigorously stirred for 24 h. In the end, the as-prepared precipitates were collected, washed with deionized water and dried at 60 ^oC for 24 h.

To prepare heterostructure 5% $Ag/AgCl/Bi_2MoO_6$ nanocomposites by sonochemical-assisted deposition method, 5% $AgNO_3$ by weight was dissolved in 100 ml ethylene glycol as reducing reagent, followed by adding of 2.5 g of the as-prepared heterostructure 5% $AgCl/Bi_2MoO_6$ nanocomposites and continued to be stirred for 30 min. Then, the whole system was transferred in ultrasonic bath and irradiated by ultrasonic wave for 20 min. In the end, the as-prepared precipitates were collected, washed with deionized water three times and dried for further characterization by an X-ray diffractometer (XRD), a scanning electron microscope (SEM) with a connected energy dispersive X-ray spectrometer (EDS) and X-ray photoelectron spectroscopy (XPS).

Photocatalytic activity of photocatalyst was investigated through the photodegradation of RhB under visible light irradiation ($\lambda \geq 420$ nm). The 0.2 g photocatalyst was weighted and suspended in 200 ml of $1x10^{-5}$ M RhB solution under stirring in the dark for 30 min. At the end of visible light illumination, the RhB solution was collected at a given time interval and centrifuged to remove the photocatalytic solid. The residual concentration of RhB after photocatalytic reaction was measured at the maximum absorption of RhB at 554 nm by UV–visible spectroscopy. The decolorization efficiency was calculated as follows.

$$\text{Decolorization efficiency (\%)} = \frac{C_o - C_t}{C_o} \times 100 \quad (1)$$

where C_o is the initial concentration of RhB and C_t is the concentration of RhB after light irradiation.

3. Results and discussion

Fig. 1 shows X-ray diffraction (XRD) patterns of as-prepared Bi_2MoO_6, $AgCl/Bi_2MoO_6$ and $Ag/AgCl/Bi_2MoO_6$ samples. The XRD pattern of the pure Bi_2MoO_6 sample synthesized by simple hydrothermal method represents the sharp diffraction peaks at $2\theta = 10.92^o$, 28.27^o, 32.20^o, 32.62^o, 33.13^o, 36.03^o, 46.21^o, 46.71^o, 47.20^o, 55.58^o, 56.23^o and 58.48^o. They can be indexed to the (020), (131), (200), (002), (060), (151), (152), (202), (260)/(062), (133), (191) and (262) planes of orthorhombic phase of Bi_2MoO_6 structure (JCPDS No. 21-0102 [23]). No impurity has been detected from the diffraction pattern. The XRD pattern of heterostructure $AgCl/Bi_2MoO_6$ nanocomposites shows new diffraction peaks at $2\theta = 27.83^o$, 32.23^o and 46.27^o which can be indexed to (111), (200) and (220) planes of cubic AgCl phase which is in accordance with those of the JCPDS No. 31-1238 [23], indicating the formation of AgCl and Bi_2MoO_6 with a good crystallinity. These nanocomposites are the mixed phases of orthorhombic Bi_2MoO_6 structure as major phase and cubic AgCl as minor phase. The XRD pattern of heterostructure $Ag/AgCl/Bi_2MoO_6$ nanocomposites show a weak peak at $2\theta = 38.16^o$ which can be indexed to the (111) plane of face center cubic (FCC) metallic Ag (JCPDS No. 87-0717 [23]), demonstrating that Ag^+ ions were reduced to metallic Ag and deposited on the surface of $AgCl/Bi_2MoO_6$ nanocomposites [24, 25]. No detection of characteristic peaks of impurities in the pattern, indicating that the obtained heterostructure $Ag/AgCl/Bi_2MoO_6$ nanocomposites were composed of metallic Ag, AgCl and Bi_2MoO_6.

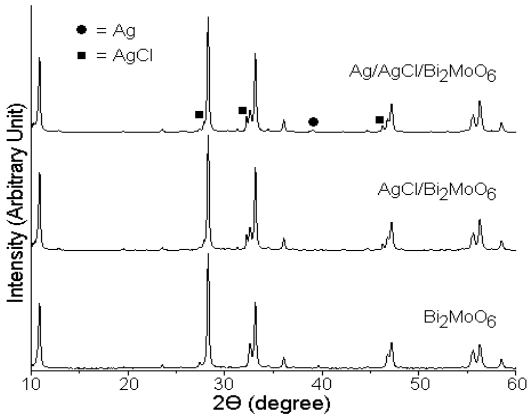

Fig. 1. XRD patterns of Bi_2MoO_6, $AgCl/Bi_2MoO_6$ and $Ag/AgCl/Bi_2MoO_6$.

The morphologies of as-prepared samples were analyzed by a scanning electron microscope (SEM). The pure Bi_2MoO_6 sample (Fig. 2a and b) presents a lot of nanoplates with an average diameter of 0.5-0.8 μm. The surfaces of Bi_2MoO_6 nanoplates were smooth. Fig. 2c and d shows the SEM images of $AgCl/Bi_2MoO_6$ nanoplates with rough surfaces. They can be seen that AgCl nanoparticles with the size of 10-20 nm supported in the surface of Bi_2MoO_6 nanoplates. The $Ag/AgCl/Bi_2MoO_6$ nanocomposites (Fig. 2e and f) show both of Ag and AgCl nanoparticles with less than 20 nm decorated on the surface of Bi_2MoO_6 nanoplates. The elemental composition of the $Ag/AgCl/Bi_2MoO_6$ composites was measured using energy-dispersive X-ray (EDS) spectroscopy (Fig. 3). The EDS mapping analysis of $Ag/AgCl/Bi_2MoO_6$ composites shows Ag, Cl, Bi, Mo and O containing in the composites which confirmed the good distribution of Ag and AgCl nanoparticles on the surface of Bi_2MoO_6 nanoplates.

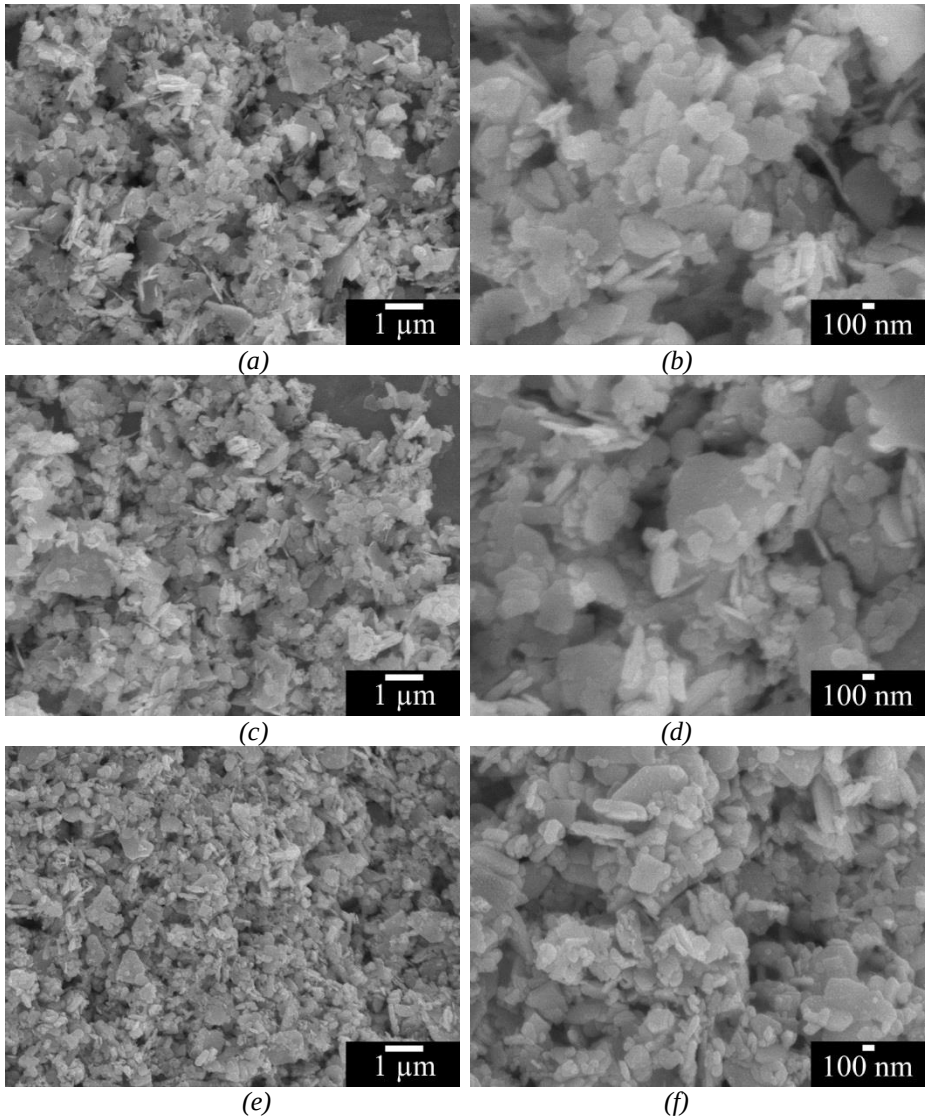

Fig. 2. SEM images at low and high magnifications of (a and b) Bi_2MoO_6, (c and d) $AgCl/Bi_2MoO_6$ and (e and f) $Ag/AgCl/Bi_2MoO_6$ nanocomposites.

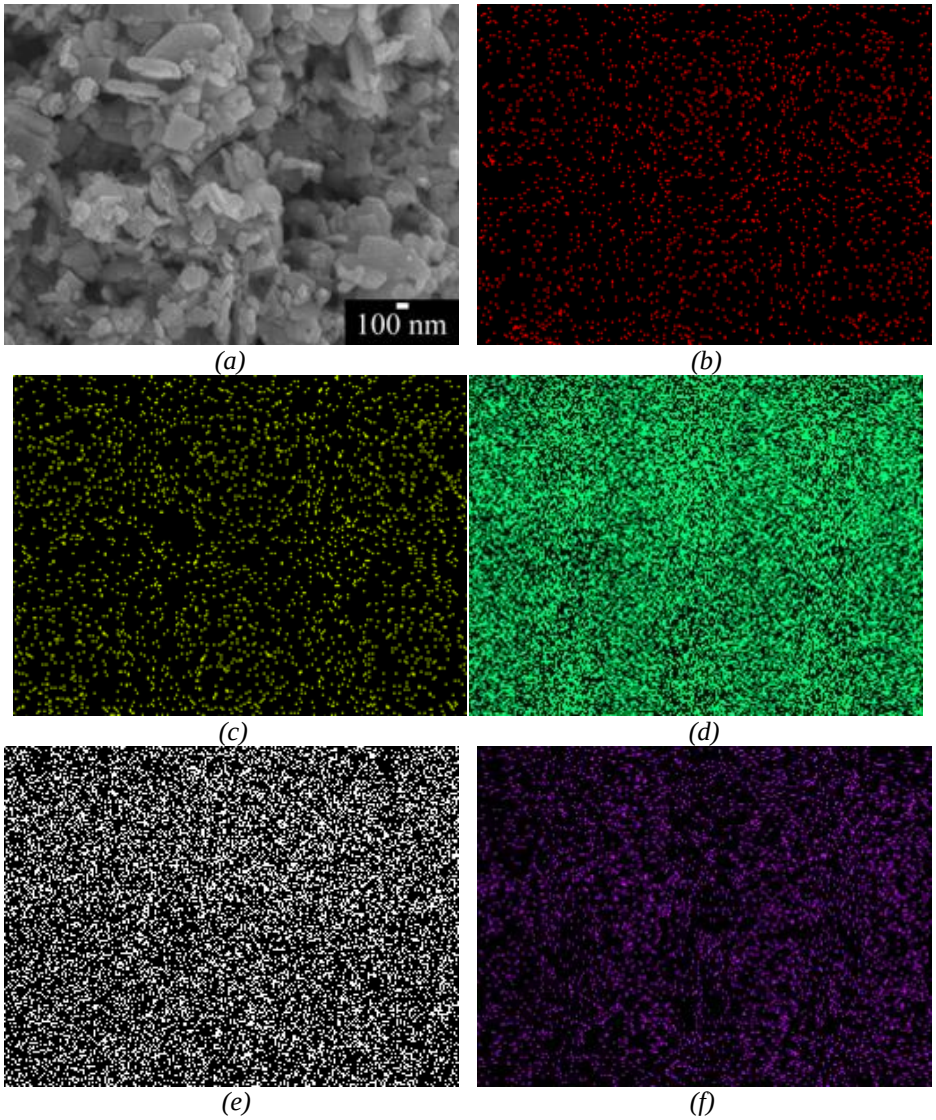

Fig. 3. (a) SEM image and EDS mapping of (b) Ag, (c) Cl, (d) Bi, (e) Mo and (f) O of as-prepared Ag/AgCl/Bi_2MoO_6 nanocomposites.

The optical properties of Bi_2MoO_6 and Ag/AgCl/Bi_2MoO_6 nanocomposites have been investigated by UV-visible spectroscopy (Fig. 4). The UV-visible absorption of Bi_2MoO_6 shows the good absorption in UV-visible region with the absorption edge of 425 nm [6, 7, 13, 15, 22]. The Ag/AgCl/Bi_2MoO_6 sample has visible light absorption higher than pure Bi_2MoO_6 nanoplates. The absorption edge of Ag/AgCl/Bi_2MoO_6 composites was red-shifted to 439 nm, indicating that the Ag/AgCl/Bi_2MoO_6 composites as photocatalyst can absorb the wider range of photonic light during photocatalytic reaction [13, 15, 22]. Therefore, the deposition of Ag/AgCl nanoparticles on the nanoplates are the benefit of Bi_2MoO_6 photocatalyst to absorb visible radiation.

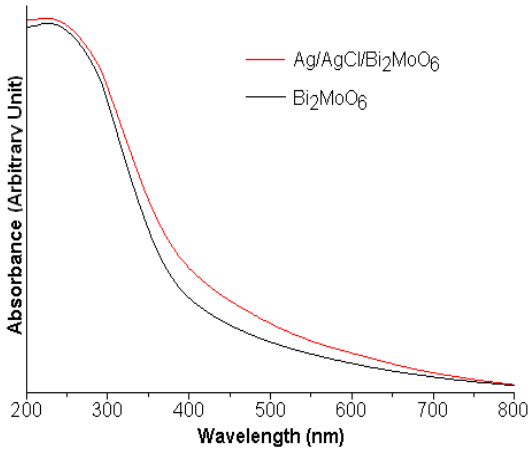

Fig. 4. UV-visible spectra of as-prepared Bi_2MoO_6 and Ag/AgCl/Bi_2MoO_6 samples.

X-ray photoelectron spectroscopic (XPS) analyzer was used to analyze the elemental composition and chemical state of the as-prepared Ag/AgCl/Bi_2MoO_6 nanocomposites. The survey spectrum of the as-prepared Ag/AgCl/Bi_2MoO_6 nanocomposites (Fig. 5a) shows the binding energies of C, Ag, Cl, Bi, Mo and O core levels of the composites. The C element was attributed to the adventitious hydrocarbon from the XPS instrument itself. The high-resolution binding energies spectra of Ag 3d, Cl 2p, Bi 4f, Mo 3d and O 1s core levels are also displayed. Fig. 5b shows the high-resolution binding energies of Ag core levels which can be further deconvoluted into two peaks at about 367.18/368.03 eV for Ag $3d_{5/2}$ and 373.16/373.89 eV for Ag $3d_{3/2}$ core levels [13, 15, 16, 20, 21]. The binding energy peaks located at 367.18 eV and 373.16 eV were attributed to Ag $3d_{5/2}$ and Ag $3d_{3/2}$ core levels of Ag^+, whereas the binding energy peaks located at 368.03 eV and 373.89 eV were attributed to Ag $3d_{5/2}$ and Ag $3d_{3/2}$ core levels of Ag^0, indicating that the Ag species containing in Ag/AgCl/Bi_2MoO_6 are the mixture of Ag^+ from AgCl and metallic FCC Ag^0 [1, 2, 13, 15, 16, 20, 21]. Fig. 5c shows the binding energy peaks of Cl 2p core levels at 198.01 eV and 199.78 eV which are attributed to Cl $2p_{3/2}$ and $2p_{1/2}$ core levels, respectively. Thus, the oxidation state of Cl is Cl^- ions of AgCl [1, 15, 16, 20]. Two symmetric binding energy peaks at 159.23 eV and 164.54 eV were detected by XPS (Fig. 5d) and are ascribed to the Bi $4f_{7/2}$ and Bi $4f_{5/2}$ core levels of Bi^{3+} [2, 6, 7, 11, 15]. Fig. 5e shows two binding energy peaks located at 232.52 eV and 235.66 eV which are ascribed to Mo $3d_{5/2}$ and Mo $3d_{3/2}$ of Mo^{6+}, respectively [2, 6, 7, 11, 15]. In addition, the asymmetric binding energies of O 1s peak of Ag/AgCl/Bi_2MoO_6 nanocomposites (Fig. 5f) can be deconvoluted into four peaks at 530.05 eV, 531.05 eV, 532.15 eV and 533.33 eV which are ascribed to oxygen of Bi–O, Mo–O bonds and surface-adsorbed oxygen [2, 6, 7, 11]. Thus, the XPS analysis confirms the existence of metallic Ag^0 and AgCl containing in the Ag/AgCl/Bi_2MoO_6 nanocomposites and is in accordance with the above XRD analysis.

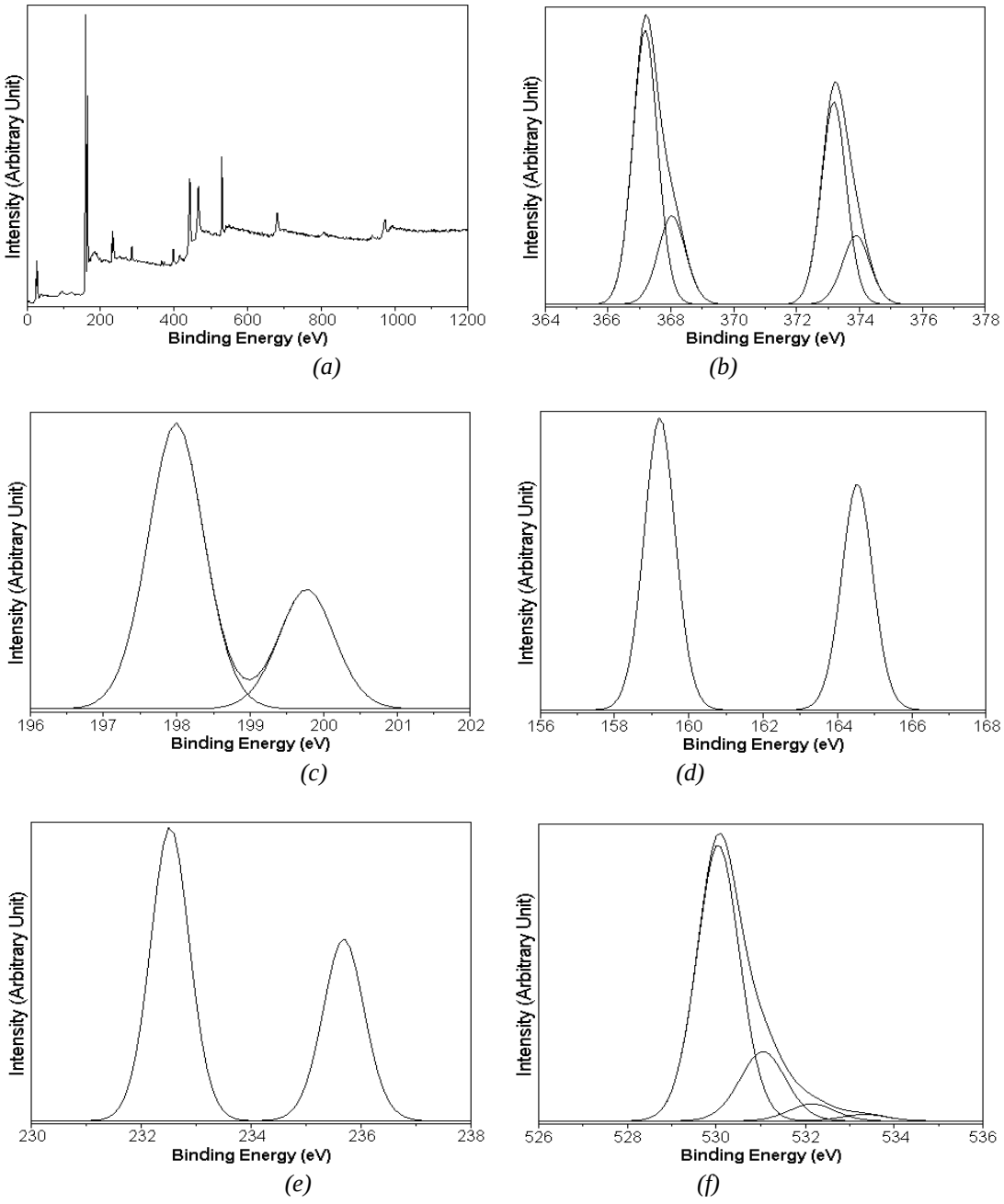

Fig. 5. XPS spectra of (a) full scan, (b) Ag 3d, (c) Cl 2p, (d) Bi 4f, (e) Mo 3d and (f) O 1s of as-prepared Ag/AgCl/Bi_2MoO_6 nanocomposites.

The photocatalytic activities of as-prepared pure Bi_2MoO_6, AgCl/Bi_2MoO_6 and Ag/AgCl/Bi_2MoO_6 composites were evaluated through the degradation of RhB under visible light irradiation ($\lambda > 420$ nm). Fig. 6 shows the temporal evolution of the UV-visible absorption spectral change of RhB solution containing Bi_2MoO_6, AgCl/Bi_2MoO_6 and Ag/AgCl/Bi_2MoO_6 nanocomposites under visible light irradiation within 0-30 min. The photocatalytic degradation results showed the continuous decrease of main absorption peaks of RhB solution at 554 nm over Bi_2MoO_6, AgCl/Bi_2MoO_6 and Ag/AgCl/Bi_2MoO_6 nanocomposites under visible light irradiation with the

increase of irradiation time. These results show that the dye molecules were mineralized due to the photocatalytic behavior of the synthesized material [11, 13, 20]. Among them, the Ag/AgCl/Bi_2MoO_6 nanocomposites have the fastest decrease of absorption peak of RhB solution under visible light irradiation. Clearly, the absorption peak of RhB located at 554 nm was gradually blue-shifted to 498 nm within 30 min by N-deethylation of RhB [11, 13, 26, 27]. After 30 min testing, the absorption peak of RhB was decreased by degradation process and the pink color was no longer detected.

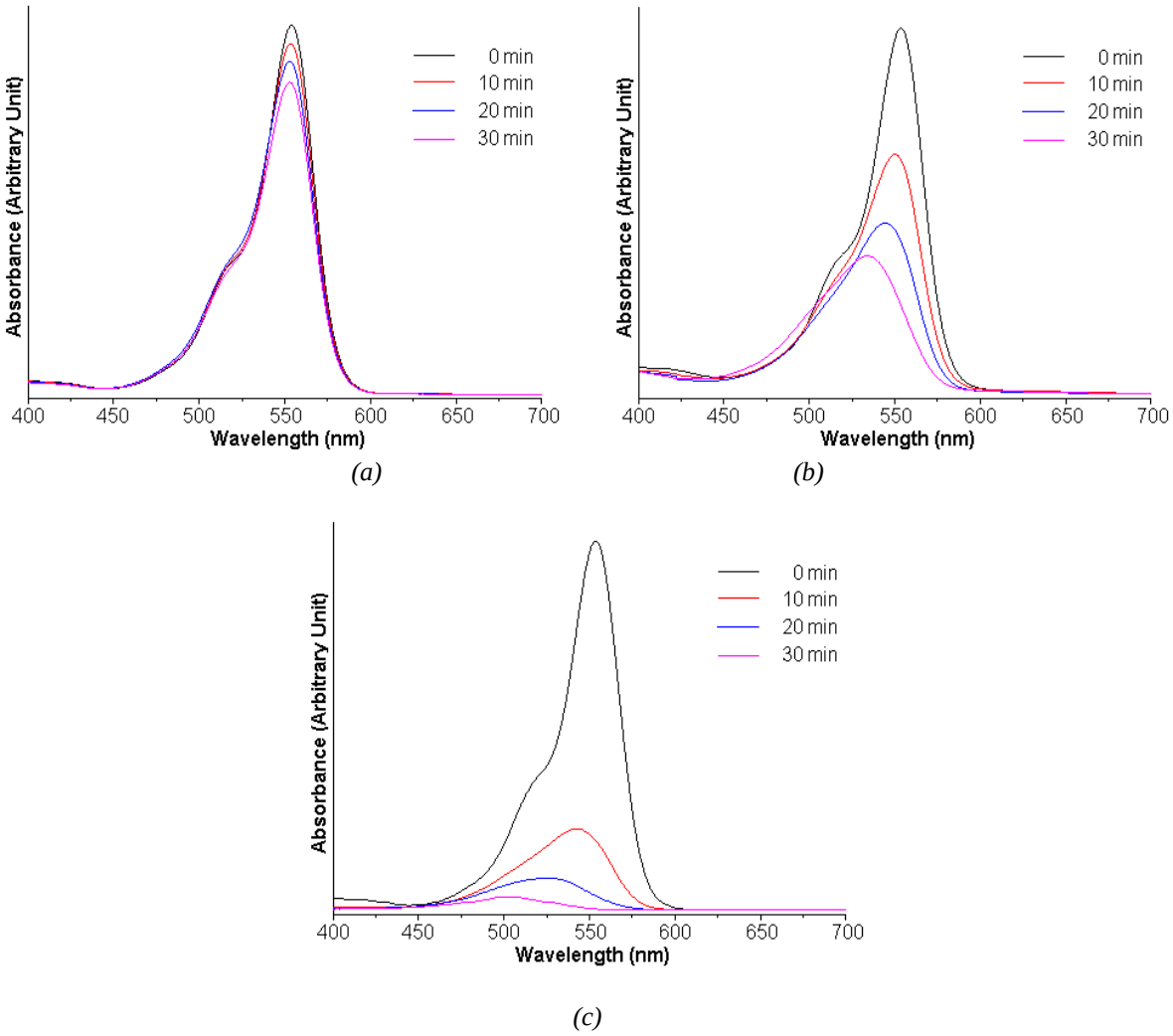

Fig. 6. UV-visible spectra of RhB over (a) Bi_2MoO_6, (b) AgCl/Bi_2MoO_6 and (c) Ag/AgCl/Bi_2MoO_6 under visible light irradiation.

The photocatalytic activities of fabricated photocatalysts were determined and compared. Fig. 7a shows the photocatalytic performance of pure Bi_2MoO_6, AgCl/Bi_2MoO_6 and Ag/AgCl/Bi_2MoO_6 nanocomposites in degrading RhB under visible light irradiation. The Ag/AgCl/Bi_2MoO_6 composites have photocatalytic performance in degrading RhB higher than pure Bi_2MoO_6 and AgCl/Bi_2MoO_6 nanocomposites. The photocatalytic efficacies of Bi_2MoO_6, AgCl/Bi_2MoO_6 and Ag/AgCl/Bi_2MoO_6 were 15.63%, 75.78% and 99.70% under visible light irradiation within 30 min, respectively. This result indicated that the Ag/AgCl nanoparticles deposited

on surface of Bi_2MoO_6 nanoplates have the great influence on the photocatalytic activity of Bi_2MoO_6 [1, 13, 15-17, 20, 22]. The kinetics of photocatalytic performance of pure Bi_2MoO_6, $AgCl/Bi_2MoO_6$ and $Ag/AgCl/Bi_2MoO_6$ nanocomposites under visible light irradiation were studied using the Langmuir-Hinshelwood model as follows.

$$\ln(C_0/C_t) = kt \quad (2)$$

where C_0 and C_t are the initial concentration and the concentration at each specific reaction time of RhB and k is the reaction rate constant [1, 6, 7, 9, 11]. Fig. 7b showed the $\ln(C_0/C_t)$ versus time (t) plots for RhB degradation over pure Bi_2MoO_6, $AgCl/Bi_2MoO_6$ and $Ag/AgCl/Bi_2MoO_6$ nanocomposites under visible light irradiation. The plots show the linear lines of $\ln(C_0/C_t)$ versus time (t) plot of RhB degradation over all photocatalysts with R^2 closed to 1.00, indicating that the RhB degradation over pure Bi_2MoO_6, $AgCl/Bi_2MoO_6$ and $Ag/AgCl/Bi_2MoO_6$ nanocomposites under visible light irradiation is pseudo first order kinetics [6, 11, 26, 27]. The rate constants for RhB degradation over pure Bi_2MoO_6, $AgCl/Bi_2MoO_6$ and $Ag/AgCl/Bi_2MoO_6$ nanocomposites under visible light irradiation were $5.83x10^{-3}$, 0.0472 and 0.1847 min^{-1}, respectively due to the increase of effectively photo-generated electrons and holes separation by the excellent conductive properties of Ag nanoparticles and energy level matching with that of AgCl and Bi_2MoO_6 [1, 13, 15-17, 20, 22].

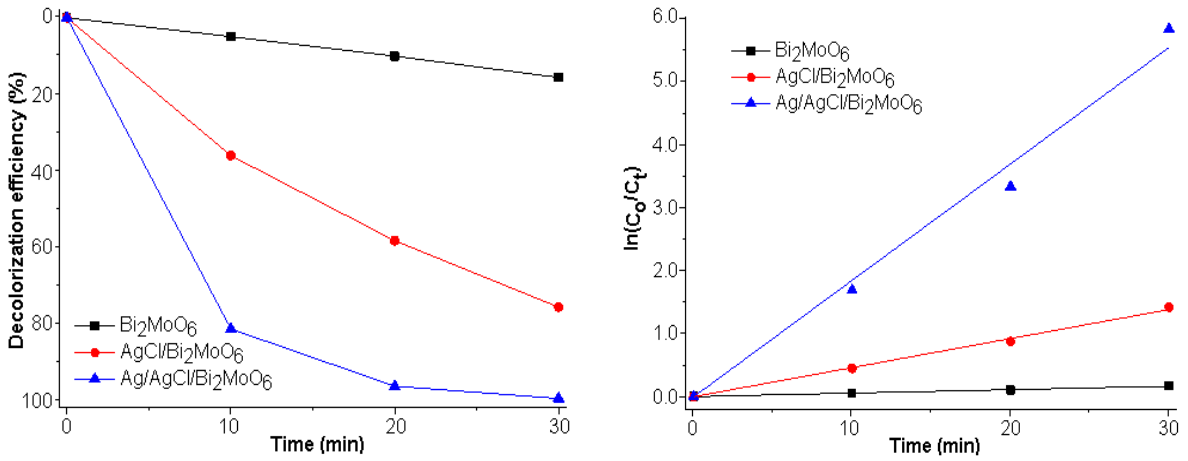

(a) *(b)*

Fig. 7. (a) Decolorization efficiency and (b) first-order plots for the photocatalytic degradation of RhB over Bi_2MoO_6, $AgCl/Bi_2MoO_6$ and $Ag/AgCl/Bi_2MoO_6$ under visible light irradiation.

The photocatalytic performance of $Ag/AgCl/Bi_2MoO_6$ nanocomposites in degrading RhB under visible light irradiation was studied by different active scavenger adding such as triethanolamine (TEOA), benzoquinone (BQ) and isopropyl alcohol (IPA) for hole (h^+), superoxide ($^{\bullet}O_2^-$) and hydroxyl ($^{\bullet}OH$) radical scavengers, respectively [1, 5, 12, 17, 28, 29]. Fig. 8a shows the influence of active scavenger species on photodegradation of RhB over $Ag/AgCl/Bi_2MoO_6$ nanocomposites under visible light irradiation. In this research, the photocatalytic efficiencies in degrading RhB were suppressed to 22.57% and 15.32% in the presence of TEOA and BQ scavengers, respectively. When IPA was added to the photocatalytic reaction solution, the photodegradation of RhB solution has a little decrease rate relative to that of RhB solution without a scavenger. Therefore, h^+ and $^{\bullet}O_2^-$ radicals played the important role in degrading RhB over $Ag/AgCl/Bi_2MoO_6$ nanocomposites under visible light irradiation more than $^{\bullet}OH$ radical [1, 15, 16, 22].

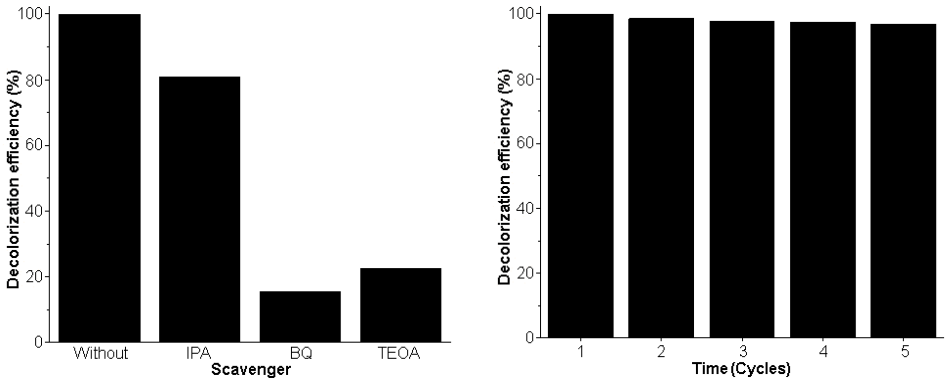

Fig. 8. (a) Effect of different scavengers and (b) reused five-cycled Ag/AgCl/Bi_2MoO_6 nanocomposites in degrading RhB under visible light irradiation.

The stability of a photocatalyst is very important for the Ag/AgCl/Bi_2MoO_6 nanocomposites which were reused for five cycles. Thus, the photodegradation experiment was done to investigate the stability of the photocatalyst for practical application. Fig. 8b shows the photocatalytic performance of Ag/AgCl/Bi_2MoO_6 nanocomposites in degrading RhB under visible light irradiation for five recycles. The photocatalytic activity of reused Ag/AgCl/Bi_2MoO_6 nanocomposites was slightly decreased from 99.70% for the 1st cycle to 96.50% for the 5th cycle. The result indicates the excellent reusable performance of Ag/AgCl/Bi_2MoO_6 nanocomposites under visible light irradiation. The phase of reused Ag/AgCl/Bi_2MoO_6 nanocomposites after degrading RhB for five cycles was investigated by XRD as the results shown in Fig. 9. In this research, the phase and structure of Ag/AgCl/Bi_2MoO_6 nanocomposites were not changed after the reuse of the fifth cycle. Furtherly, these results verify that the photocatalyst has excellent stability and recyclability.

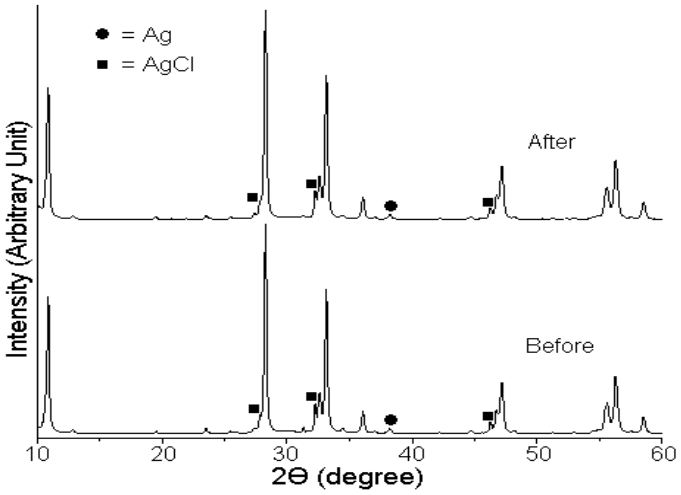

Fig. 9. XRD patterns of Ag/AgCl/Bi_2MoO_6 nanocomposites before and after reuse of the fifth cycle.

4. Conclusions

In summary, heterostructure Ag/AgCl/Bi_2MoO_6 nanocomposites as visible-light-driven photocatalyst were successfully synthesized by precipitation and sonochemical deposition method and were used for photodegradation of RhB under visible light irradiation. The nanocomposites have the degradation of RhB under visible light irradiation better than pure Bi_2MoO_6 sample and AgCl/Bi_2MoO_6 nanocomposites due to the increase of effectively photo-generated electrons and holes separation rate by the excellent conductive properties of Ag nanoparticles and energy level matching of AgCl and Bi_2MoO_6. The photocatalytic stability of Ag/AgCl/Bi_2MoO_6 nanocomposites show slight decrease of photodegradation of RhB under visible light irradiation, including the excellent reusable performance of Ag/AgCl/Bi_2MoO_6 nanocomposites under visible light irradiation.

Acknowledgements

This research was supported by National Science, Research and Innovation Fund and Prince of Songkla University (Grant No TAE6505097M), Thailand.

References

[1] S. F. Yang, C. G. Niu, D. W. Huang, H. Zhang, G. M. Zeng, J. Colloid Interf. Sci. 505, 96 (2017). https://doi.org/10.1016/j.jcis.2017.05.108

[2] V. Shanmugam, A. L. Muppudathi, S. Jayavel, K. S. Jeyaperumal, Arab. J. Chem. 13, 2439 (2020); https://doi.org/10.1016/j.arabjc.2018.05.009

[3] J. Wang, X. H. Sun, H. Du, Russ. J. Inorg. Chem. 65, 1111 (2020); https://doi.org/10.1134/S0036023620070244

[4] C. Peng, Y. Liu, J. Cui, Y. Shen, Dig. J. Nanomate. Bios. 15, 991 (2020).

[5] Q. Shen, M. H. Xu, G. X. Pan, S .L. Lai, Y. H. Tong, Dig. J. Nanomater. Bios. 16, 271 (2021).

[6] P. Dumrongrojthanath, A. Phuruangrat, S. Thongtem, T. Thongtem, J. Iran. Chem. Soc. 16, 733 (2019); https://doi.org/10.1007/s13738-018-1550-5

[7] J. Wang, Y. Sun, Z. Wang, C. Wu, P. Rao, Russ. J. Phys. Chem. A 93, 736 (2019); https://doi.org/10.1134/S0036024419040307

[8] Y. Tan, C. Yin, S. Zheng, Y. Di, Z. Sun, C. Li, Appl. Clay Sci. 215, 106319 (2021); https://doi.org/10.1016/j.clay.2021.106319

[9] P. Intaphong, A. Phuruangrat, K. Lertwittayanon, K. Akbhari, S. Thongtem, T. Thongtem, Dig. J. Nanomater. Bios. 16, 175 (2021).

[10] M. Li, D. Li, Z. Zhou, P. Wang, X. Mi, Y. Xia, H. Wang, S. Zhan, Y. Li, L. Li, Chem. Eng. J. 382, 122762 (2020); https://doi.org/10.1016/j.cej.2019.122762

[11] A. Phuruangrat, T. Klangnoi, P. Patiphatpanya, P. Dumrongrojthanath, S. Thongtem, T. Thongtem, Optik 212, 164674 (2020); https://doi.org/10.1016/j.ijleo.2020.164674

[12] W. Chen, G. R. Duan, T. Y. Liu, S. M. Chen, X. H. Liu, Mater. Sci. Semicond. Process. 35, 45 (2015).

[13] Q. Yan, M. Sun, T. Yan, M. Li, L. Yan, D. Wei, B. Du, RSC Adv. 5, 17245 (2015); https://doi.org/10.1039/C4RA15821K

[14] P. Guo, X. Hu, M. Wang, Optik 222, 165399 (2020); https://doi.org/10.1016/j.ijleo.2020.165399

[15] X. Li, S. Fang, L. Ge, C. Han, P. Qiu, W. Liu, Appl. Catal. B 176-177, 62 (2015);

https://doi.org/10.1016/j.apcatb.2015.03.042
[16] R. Yang, F. Dong, X. You, M. Liu, S. Zhong, L. Zhang, B. Liu, Mater. Lett. 252, 272 (2019); https://doi.org/10.1016/j.matlet.2019.06.006
[17] C. Chai, J. Liu, Y. Wang, X. Zhang, D. Duan, C. Fan, Y. Wang, Appl. Phys. A 125, 96 (2019); https://doi.org/10.1007/s00339-019-2384-4
[18] L. Xie, A. Li, S. Zhou, M. Zhang, Y. Ding, P. Wang, Res. Chem. Intermed. 47, 2373 (2021).
[19] T. He, D. Wu, J. Mater. Sci. 28, 7320 (2017); https://doi.org/10.1007/s10854-017-6418-4
[20] W. Liu, S. Hu, Y. Wang, B. Zhang, R. Jin, L. Hu, Nanoscale Res. Lett. 14, 108 (2019); https://doi.org/10.1186/s11671-019-3055-2
[21] H. He, J. Li, C. Yu, Z. Luo, Sustain. Mater. Technol. 22, e00127 (2019); https://doi.org/10.1016/j.susmat.2019.e00127
[22] J. Zhang, C. Niu, J. Ke, L. Zhou, G. Zeng, Catal. Commun. 59, 30 (2015); https://doi.org/10.1016/j.catcom.2014.09.041
[23] Powder Diffract. File, JCPDS-ICDD, 12 Campus Boulevard, Newtown Square, PA 19073-3273, U.S.A., (2001).
[24] A. Phuruangrat, P. Dumrongrojthanath, B. Kuntalue, S. Thongtem, T. Thongtem, Dig. J. Nanomater. Bios. 15, 167 (2020).
[25] V. G. Pol, D. N. Srivastava, O. Palchik, V. Palchik, M. A. Slifkin, A. M. Weiss, A. Gedanken, Langmuir 18, 3352 (2002); https://doi.org/10.1021/la0155552
[26] P. Intaphong, A. Phuruangrat, T. Thongtem, S. Thongtem, J. Aust. Ceram. Soc. 55, 1021 (2019); https://doi.org/10.1007/s41779-019-00314-w
[27] A. Phuruangrat, S. Jonjana, S. Thongtem, T. Thongtem, J. Aust. Ceram. Soc. 55, 57 (2019); https://doi.org/10.1007/s41779-018-0210-7
[28] Z. Wang, Y. Song, X. Cai, J. Zhang, T. Tang, S. Wen, R. Soc. open sci. 6, 191077 (2019); https://doi.org/10.1098/rsos.191077
[29] Z. Gou, J. Dai, J. Bai, Int. J. Electrochem. Sci. 15, 10684 (2020); https://doi.org/10.20964/2020.11.68